ELSEVIER

Earth and Planetary Science Letters 169 (1999) 37–50

EPSL

Central anomaly magnetization high: constraints on the volcanic construction and architecture of seismic layer 2A at a fast-spreading mid-ocean ridge, the EPR at 9°30′–50′N

Hans Schouten [a,*], Maurice A. Tivey [a], Daniel J. Fornari [a], James R. Cochran [b]

[a] *Department of Geology and Geophysics, Woods Hole Oceanographic Institution, Woods Hole, MA 02543, USA*
[b] *Lamont-Doherty Earth Observatory, Columbia University, Palisades, NY 10964, USA*

Received 18 May 1998; revised version received 5 February 1999; accepted 8 March 1999

Abstract

The central anomaly magnetization high (CAMH) is a zone of high crustal magnetization centered on the axis of the East Pacific Rise (EPR) and many other segments of the global mid-ocean ridge (MOR). The CAMH is thought to reflect the presence of recently emplaced and highly magnetic lavas. Forward models show that the complicated character of the near-bottom CAMH can be successfully reproduced by the convolution of a lava deposition distribution with a lava magnetization function that describes the variation in lava magnetization intensity with age. This lava magnetization function is the product of geomagnetic paleofield intensity, which has increased by a factor of 2 over the last 40 kyr, and low-temperature alteration which decreases the remanence of lava with exposure to seawater. The success of the forward modeling justifies the inverse approach: deconvolution of the magnetic data for lava distribution and integration of that distribution for magnetic layer thickness. This approach is tested on two near-bottom magnetic profiles AL2767 and AL2771, collected using *Alvin* across the EPR axis at 9°31′N and 9°50′N. Our analysis of these data produces an estimate of the relative thickness of the magnetic lava layer which is remarkably consistent with existing multichannel estimates of layer 2A thickness from lines CDP31 and CDP27. The similarity between magnetic layer and seismic layer 2A at the 9°–10°N segment of the EPR crest provides independent support to the notion that seismic layer 2A in young oceanic crust represents the highly magnetic lava layer, and that the velocity gradient at the base of layer 2A is related to the increasing number of higher-velocity dikes with depth in the lava–dike transition zone. The near-bottom magnetic anomaly character of the CAMH is a powerful indicator of the emplacement history of upper crust at MORs which allows prediction of the relative thickness and architecture of the extrusive lavas independent of other constraints.

Keywords: mid-ocean ridges; East Pacific Rise; magnetic anomalies; seismic stratigraphy; volcanic processes

1. Introduction

Understanding how magma is supplied to the crust at a mid-ocean ridge (MOR) and the mode of its emplacement, both of which impart the basic architecture of the extrusive crustal sequence, is of primary importance if we are to understand the history of crustal accretion and volcanic stratigraphy in the vertical dimension. In recent years, geophysical studies have provided a revelation in terms of the detailed structure of the upper volcanic layer in young

* Corresponding author. Tel.: +1 508 289 2574; Fax: +1 508 457 2150; E-mail: hschouten@whoi.edu

0012-821X/99/$ – see front matter
PII: S0012-821X(99)00063-1

ocean crust. Multichannel seismic experiments have shown a ubiquitous pattern of extrusive thickening along the EPR (e.g., [1–5]). The new seismic model of layer 2A [5–9] shows that instead of reaching its full thickness at the axis, layer 2A increases to its constant thickness over a relatively short spatial interval, usually within ~2–4 km of the spreading axis. This pattern of extrusive layer thickening observed along the EPR at 9°–10°N, 14°S, and 17°S is remarkably consistent over the 110–150 mm/yr range of spreading rates [5,9,10]. On-bottom seismic refraction experiments at the EPR 9°30′N, showed a similar pattern of extrusive thickening which Christeson et al. [6] attributed to off-axis lava deposition resulting from overflow of lavas from the axial summit trough and/or off-axis eruption (e.g., [11,12]).

Current accretionary models for the EPR focus on the volcanic and hydrothermal processes occurring within the narrow (~<1 km wide) axial zone (e.g., [11,13,14]) and the predominance of volcanic effusion within this zone. Off-axis volcanism on the EPR crestal plateau has been invoked to explain the distribution of anomalously young ages [13,15] and the occurrence of fresh lava flows and constructional volcanic features well outside the axial trough [13,16,17], but these observations are too few and local in nature to assess the magnitude of a general off-axis lava deposition process. If all the volcanic products are erupted and deposited at the axis (i.e., within or proximal to the axial trough) then the thickening of seismic layer 2A is not the lithologic boundary between sheeted dikes and extrusive lavas as assumed, but might be an alteration front. We believe however that lava deposition occurs both at the axis and up to several kilometers on either side of it and that seismic layer 2A does reflect the doubling in thickness of the extrusive lava sequence. Past studies of magnetic anomaly transition widths [18–20] have estimated the width of the neovolcanic zone to between 1 and 4 km for fast spreading mid-ocean ridges such as the EPR. This is consistent with the emerging evidence from seismic data, detailed age dating and seafloor observations. In this paper, we seek to extend the early magnetic studies by focusing on the CAMH anomaly, to understand the source of this anomaly and how the detailed structure of this anomaly may provide even tighter constraints on the distribution of lava emplacement at a fast spreading MOR.

2. The central anomaly magnetization high (CAMH)

The CAMH is a zone of high crustal magnetization centered on the spreading axis of the EPR and is a common feature of many other MOR systems [21]. Near-bottom magnetic measurements of the CAMH indicate the width of this zone is roughly between 4 and 6 km and is not dependent on spreading rate (e.g., [22]). The CAMH is thought to reflect the presence of recently emplaced and highly magnetic lavas which record both the recent doubling of the geomagnetic field intensity [23] and magnetization decay by low-temperature alteration [21,24]. Together these lead to a rapid, 5–6 fold reduction in lava magnetization over the past ~40 kyr [25]. The width of the CAMH is thus a first order estimate of the width of the axial neovolcanic zone. Furthermore, the structure of the CAMH should provide important insight into the processes of upper crustal accretion and neovolcanic architecture at MORs.

2.1. Characteristics of the near-bottom CAMH

Numerous near-bottom studies find that there is detailed character in the CAMH profile, most notably the presence of an axial magnetic low and quasi-symmetrical, near-axis flanking lows that may or may not be continuous along the strike of both the EPR [26] and Juan de Fuca Ridge (JDF) [27]. A magnetic low located directly over the axial valley of the Endeavor segment of the JDF has been interpreted to be due to crustal alteration [28], or layer 2A thinning [27,29]. Near-bottom studies of the CAMH over the faster spreading EPR near 20°S attribute the axial magnetic low to thermal demagnetization at the axis due to dike injection [26]. We discount the thermal demagnetization effect of a dike zone because the thermal anomaly is unlikely to exist for any significant period of time. This is supported by magnetic and heat flow studies of the 1993 eruption on the CoAxial segment of the JDF [30–33]. The origin of the near-axis flanking anomaly lows in the near-bottom CAMH is equally ambiguous (e.g., [21,26–28]). Tivey and Johnson [28] interpret the lows as being due to crustal alteration in zones of increased fracturing and fissuring, while Perram et al. [26] suggested short polarity

events such as the Laschamps as possible causes for the lows.

We propose a revised interpretation of the CAMH and its structure, which takes into account the spatial distribution of lava deposition at a MOR crest and the resultant thickening of the lava layer with age, and the effects of geomagnetic field intensity fluctuations and magnetization decay due to low temperature alteration. The essence of our hypothesis for the CAMH is that the high magnetic field values in the anomaly represent larger volumes of highly magnetized lavas younger than 20 kyr. Because the highs occur over a 4 to 6 km wide zone [22], this would imply significant lava deposition or growth of the extrusive carapace within that zone, which is consistent with seismic observations of layer 2A at the EPR. Before modeling the CAMH, we first discuss the lava magnetization intensity function that simulates the variation of crustal magnetization over the past 100 kyr. This function incorporates both magnetization decay due to low temperature alteration of the magnetic minerals, and variations in the geomagnetic field intensity which has fluctuated substantially over the past few tens of thousands of years.

2.2. High magnetization of young MORB

High magnetization in the CAMH has traditionally been attributed to the presence of initially strongly magnetized titanomagnetite in young pillow basalts [24,34]. Weathering by oxidation to less magnetic titanomaghemite decreases the magnetization of the pillows with time [35–38]. It is thought that, because high magnetization, fine-grained magnetite is more concentrated in the outer fine-grained layers of the pillows, weathering causes an initially rapid decrease in intensity of the lava [24,34].

On the basis of magnetic remanence data from basalts dredged on and near the EPR axis at 12°N, and near-bottom magnetic profiles across EPR axis at 19.5°S, Gee and Kent [25] estimate a rapid, 5–6 fold magnetization decrease with age of young MORB (55 A/m to 10 A/m) with a decay time of ~20 kyr. While other estimates of the magnetization decrease with age show longer decay times of 100 kyr [30] or more (e.g., [36,39]), these studies include data from greater age ranges and slower spreading ridges with greater age uncertainties, which would skew decay time estimates to longer periods. Johnson and Tivey [30] point out that the 100 kyr decay time underestimates the zero-age CoAxial lava flow magnetization suggesting that an initial rapid decay probably takes place faster than their 100 kyr decay estimate. Furthermore, Gee and Kent [25] show that lava magnetization decay must occur on time scales much less than 100 kyr in order for a positive CAMH to exist.

In addition to a decay of the magnetization due to low-temperature alteration, the magnetization vs. age of young submarine basalts is also proportional to the variation of the Earth's magnetic field intensity (e.g., [40,41]). This variation has been clarified in recent years with improved resolution of relative paleointensity data from sedimentary sections and better dating by C^{14} and oxygen isotopes (e.g., [23,42–44]). While there are discrepancies in the fine-scale details, it is relatively clear that the intensity of the Earth's magnetic field has doubled over past several tens of thousands of years [23], which constitutes a considerable signal that cannot be ignored. If paleointensity decreases by a factor 2, but the observed magnetization of young basalts decreases 5–6 fold on a similar time-scale [25], then a ~3-fold decay is due to low-temperature alteration. This implies that except for the recent increase of the geomagnetic field intensity, older intensity variations are rapidly attenuated by the decay due to low-temperature alteration. In Fig. 1 we demonstrate how, over the past 200 kyr, the magnetization of young submarine basalts can be considered a 40 kyr-old 'spike' caused by the recent doubling of the paleofield intensity and further enhanced by a three-fold decay of this magnetization due to low-temperature alteration. The narrowness of this spike and the attenuation of older paleofield variations implies that the near-bottom CAMH anomalies predominantly reflect variations in the volume of young, highly magnetized MORB rather than variations in the paleointensity of the Earth's magnetic field. This is different from the conclusions of Gee et al. [41] who suggest, based on sea surface magnetic data, that paleointensity variations are a prime cause of the CAMH. Sea-surface magnetic data, however, have limited resolution (e.g., [45]). The true nature of the short-wavelength CAMH is more accurately observed in near-bottom surveys.

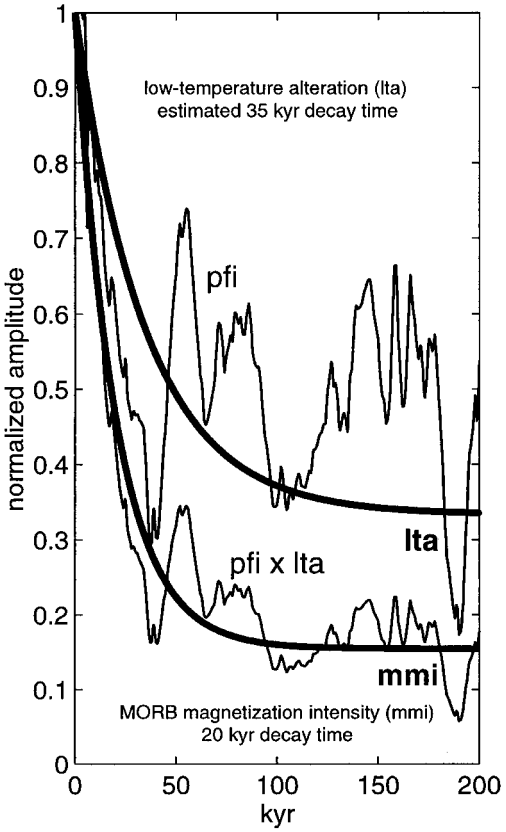

Fig. 1. Plot showing a normalized version of the sint200 relative geomagnetic paleofield intensity (*pfi*) curve of Guyodo and Valet [23] and an estimated low-temperature alteration (*lta*) curve with a decay time of 35 kyr. The product of these two variations (pfi × lta) is essentially what is being approximated when decay curves are fitted to measured NRM values of mid-ocean ridge basalts (*MORB*). We have chosen the lta curve so that the pfi × lta curve fits the ~20 kyr decay curve for the MORB magnetization intensity (*mmi*) as computed by Gee and Kent [25].

2.3. Forward models of the CAMH

We illustrate our revised interpretation with forward models of the CAMH width and structure. We use a linear, one-dimensional approximation to the process of lava deposition and magnetic anomaly generation at a MOR (e.g., [46]). Magnetic moment $M(x)$ is the convolution of the lava magnetization intensity function $I(x)$ with the lava deposition function $L(x)$, or:

$$M(x) = I(x) \times L(x) \quad \text{for} \quad x \geq 0$$

where the asterisk denotes convolution. Following Gee and Kent [25], we assume that the magnetization intensity of the young lavas decays exponentially with age to a constant background level and has the general form:

$$I(x) = (I_0 - I_\infty) \cdot \exp(-x/\tau \cdot \text{hsr}) + I_\infty$$

where I_0 is the zero-age magnetization intensity, I_∞ is the background magnetization intensity level, τ is the exponential decay time, and hsr is the half spreading rate. We use this function to model the effect of lava deposition distribution upon the near-bottom CAMH magnetic anomaly. The thickness of the lava layer $T(x)$ is uniquely determined by the lava deposition distribution $L(x)$ because:

$$T(x) = \int_0^\infty L(x)\,\mathrm{d}x$$

In Fig. 2 we show three different lava deposition distributions to simulate the characteristic 'triangle', 'bell', and 'trapezoid' shapes of layer 2A thickening observed at the EPR [4]. The axial magnetic low is caused by the narrow (<100–200 m wide) non-magnetic dike keel rising to the seafloor beneath the axis. This dike keel should be narrower than a seismic wavelength to remain invisible in the seismic layer 2A structure [9]. The models show a direct relationship between the limits of recent lava deposition, the limits of 2A thickening and the width of the CAMH. They also demonstrate that for short magnetization decay constants of the order of 20 kyr, there can be significant flanking lows within a few kilometers of the axis, even in a steady state model. Longer magnetization decay constants will reduce the amplitudes of the flanking lows and highs, and will turn most of the CAMH into a long-wavelength magnetic low that reflects the thinner magnetic layer near the axis (as demonstrated already by Gee and Kent [25]). The simulations of upper crustal architecture and magnetic structure in Fig. 2 are uniquely determined by the lava deposition distribution function and the lava magnetization intensity function.

3. Testing the CAMH Hypothesis at the EPR 9°–10°N

In Fig. 3, a reduced-to-the-pole, sea-surface magnetic anomaly map of the EPR between 9°25′N and

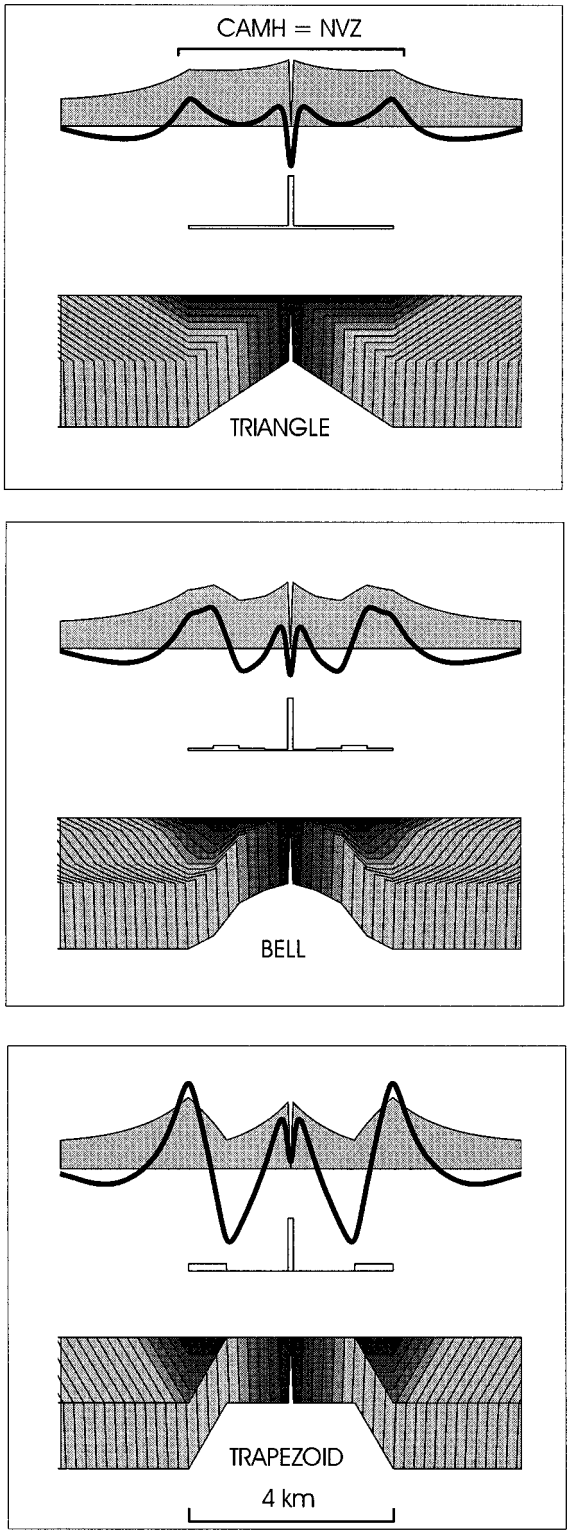

9°55′N shows the continuity and variation of the CAMH along the strike of the rise axis. The width at half the anomaly amplitude (at the +50 or +100 nT contour) is 3–5 km, suggesting a neovolcanic zone of approximately that width. Characteristically, the CAMH over the axis segment north of the 9°37′N DEVAL (deviation of axial linearity of Langmuir et al. [47]) has mostly a single maximum, while the southern segment down to 9°28′N has mostly a double maximum. While this subtle change in sea surface magnetic anomaly character would not be significant on its own because of noise problems in low latitudes, we can correlate this subtle change with a clear difference in near-bottom magnetic profiles AL2771 and AL2767 observed in these two areas (Figs. 3 and 4). Furthermore, this magnetic difference is also reflected in the thickness of seismic layer 2A on CDP27 and CDP31 (Figs. 3 and 4). Both types of observations suggest a different distribution of young lavas, or a different mode of volcanic construction at 9°50′N compared to 9°31′N.

Fig. 2. Forward models of the near-bottom magnetic anomaly and internal crustal architecture for three types of extrusive layer thickness variations: triangular, bell and trapezoid-shaped, after Kent et al. [4]. For each model, the top portion shows in gray the magnetic moment (magnetization times thickness) and the near-bottom magnetic anomaly (heavy line) computed at 100 m above the seafloor. The middle portion shows the lava deposition function consisting of an axial (proximal) distribution and a distal one. The bottom portion shows the extrusive lava thickness and internal architecture (i.e. isochrons) of the lava layer. The isochrons are every 4 kyr at 50 km/myr half rate. All models use the same narrow axial lava distribution less than 200 m wide. This narrow distribution generates half the lava layer thickness within 100 m from the axis (such rapid increase cannot be detected by the seismic systems typically used to image the base of layer 2A). The remaining thickness is formed by different distal lava distributions resulting in the characteristic triangle, bell and trapezoid shapes of layer 2A thickening observed at the East Pacific Rise. Magnetization of the lavas decreases exponentially with age from 55 A/m to a 10 A/m background level with a decay time of 20 kyr [25]. Highly magnetized lavas younger than 20 kyr are shown in darker gray shades. Magnetization of the sheeted dikes below the lava layer is set to zero ($\ll$1 A/m). The near-bottom central anomaly magnetic high (*CAMH*) anomalies clearly show the distribution of axial and distal lava depocenters and can be used to estimate their volume. Note that the CAMH width is equivalent to the width of the neovolcanic zone (*NVZ*) and also to the width of the lava layer thickening.

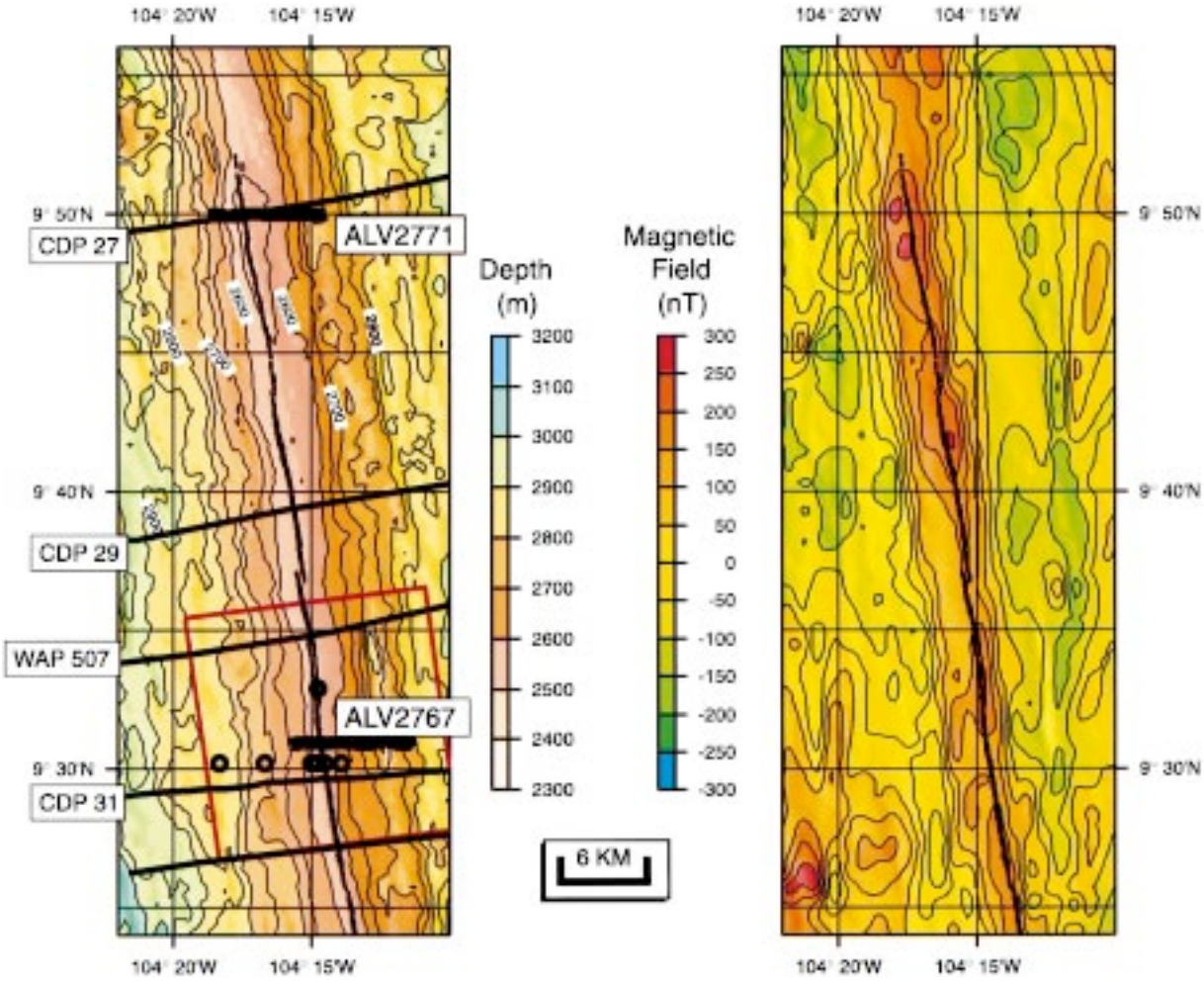

Fig. 3. Left-hand figure shows a Seabeam bathymetry map of the East Pacific Rise between 9°25′N and 9°55′N (contour interval 50 m). Bold along-axis line represents the trace of the axial summit trough [14,55]. Bold across-axis lines are multi-channel seismic lines from Vera and Diebold [2] and Harding et al. [3]; southernmost bold line is a refraction line from Christeson et al. [8], circles are on bottom refraction locations of Christeson et al. [6]. Box delineates the seismic tomography experiment of Toomey et al. [1]. Thick bold lines are *Alvin* dives from Cochran et al. [49,50]. Right-hand figure shows the sea surface magnetic field from Carbotte and Macdonald [56], reduced to the pole, showing the continuous CAMH anomaly along the axis of spreading.

3.1. Near-bottom magnetic observations of the CAMH

Magnetic profiles AL2771 and AL2767 were collected on *Alvin* dives which traversed the EPR axis and summit plateau at 9°31′N and 9°50′N [48] as part of a pilot project to collect continuous gravity measurements with a Bell gravimeter in a submersible [49,50]. The *Alvin* tracks are adjacent to multichannel seismic lines CDP27 and CDP31 which document the ubiquitous increase in thickness of layer 2A on the EPR [3].

Magnetic field data were first corrected for the magnetic effect of the submersible by using a Nelder–Meade method [51] to minimize the variation in total field observed during spins of the submersible upon descent and ascent. Typically, a 3000 nT variation was reduced by an order of magnitude to a 300 nT ripple. Magnetic field data were merged with submersible depth and altitude, and

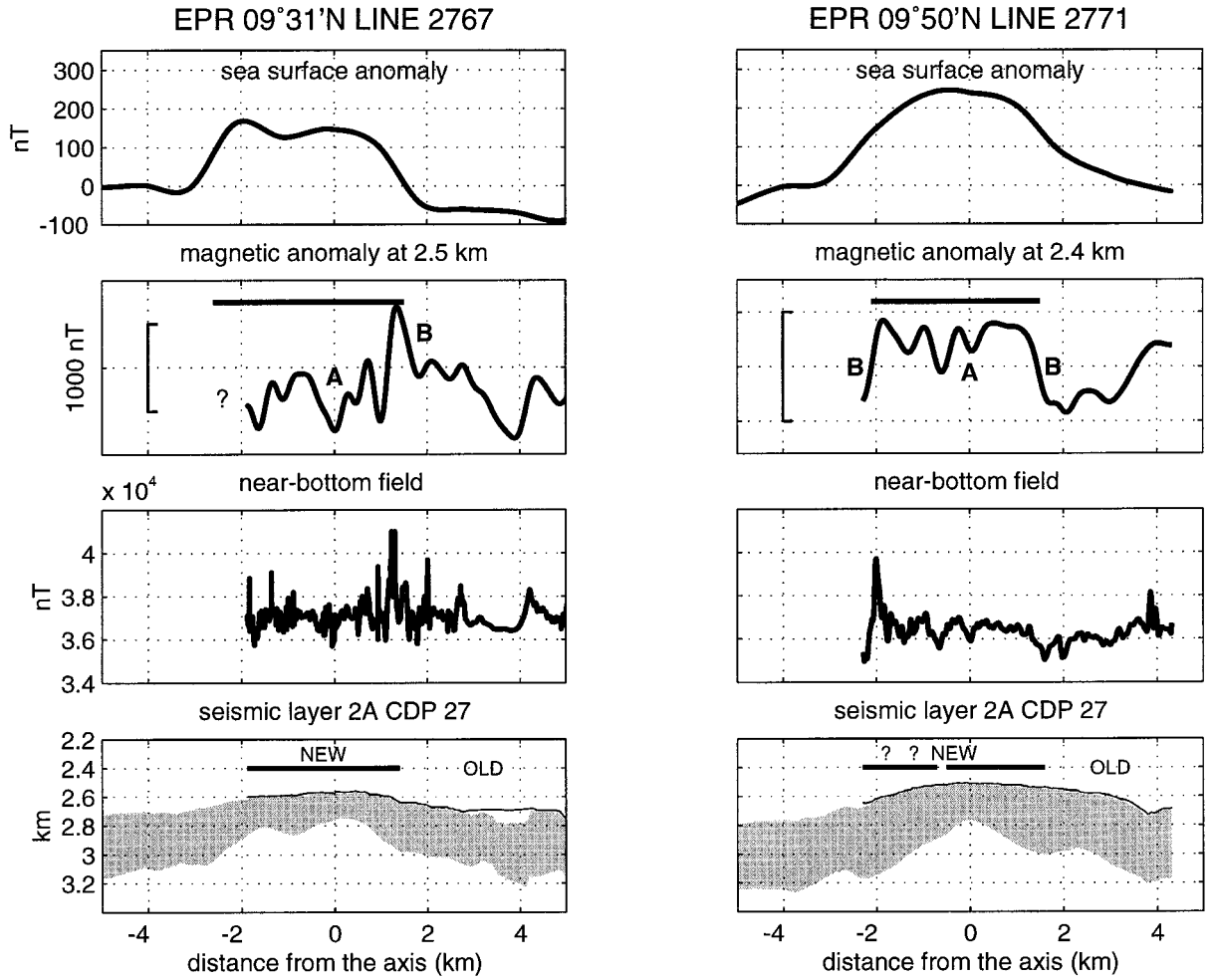

Fig. 4. Near-bottom magnetic profiles and seismic layer thickness for two *Alvin* dives identified in Fig. 3 and discussed in the text. Left hand panel shows Dive 2767 at 9°31′N [49,50]. Bottom panel shows the sea floor bathymetry and thickness of layer 2A (shaded) as determined by Harding et al. [3]. Thin line above bathymetry indicates submersible track. Bold bar above bathymetry indicates submersible observations of fresh young lava [14,49,50]. Second panel shows near-bottom magnetic anomaly field collected with *Alvin*. Third panel shows upward continued and reduced-to-the pole magnetic field at the 2.5 km level. A = axial anomaly low, B = edge anomaly, and bar shows the total extent of the CAMH. Top panel shows sea surface anomaly of Carbotte and Macdonald [56] that has been reduced to the pole (see Fig. 3). Right-hand panel shows similar data for Dive 2771 at 9°50′N [49,50]. The 2771 near-bottom magnetic field is upward continued to the 2.4 km level. Note how the limits of the CAMH (bold bar) correlate with the outer limits of observed fresh lava flows and the limits of layer 2A thickening.

then merged with *Alvin* navigation data obtained from bottom-moored acoustic transponders. Navigation accuracy and precision are in the range of 5–10 m [50]. The magnetic field data were projected along tracklines perpendicular to the rise axis and into equally spaced data points. These data were then upward continued to a level plane above the topography using the Fourier transform method of Guspi [52]. The magnetic profiles only encompass a small region, so a mean regional field was subtracted from the data calculated based on extrapolation of the 1990 DGRF model for the study area [53]. Following the traditional Fourier inversion methods of Parker and Huestis [54], we inverted the upward continued magnetic field for crustal magnetization assuming a constant thickness source layer of 0.33

km and a geocentric axial dipole field direction. This approach takes into account the topographic effects of bathymetry and the latitude dependence of anomaly phase on the magnetic signal. This approach assumes a two-dimensionality perpendicular to the profile and that the direction of magnetization is known. The crustal magnetization is converted into magnetic moment by multiplication with the 0.33 km source layer thickness.

The layer 2A structure from the seismic lines, the near-bottom CAMH, and the sea surface anomaly directly above the seismic lines (from the reduced-to-pole magnetic anomaly map in Fig. 3) are shown in Fig. 4. Both near-bottom profiles show an axial magnetic low (A in Fig. 4) and a variety of flanking lows. Overall, the two magnetic profiles in Fig. 4 are strikingly dissimilar and we propose this is caused by variations in the pattern of lava deposition in these two areas as reflected by the different layer 2A thickness variations found at the two sites [3]. Significantly, as the axis is approached, a steep magnetic gradient (edge anomaly B in Fig. 4) is present where layer 2A reaches its constant thickness; it also marks a noticeable transition from older to younger lavas [49,50]. This observation is common to both near-bottom profiles at 9°31′N and 9°50′N. At 9°50′N, observations during dive AL2768, which traversed the same track as AL2771, note a distinct change in lava terrain from the older, sedimented pillow forms to younger, clearly less sedimented, more glassy lobate flows, approximately 1.6 km east of the axis. Also, from this point west toward the axis, the summit is dominated by sparsely sedimented lobate flows and extensive collapse zones ([14], Kurras and Fornari, unpublished data). Similarly, at 9°31′N at approximately 1.4 km east of the axis, AL2767 observations note a distinct reduction in sediment cover, fresh glassy lavas and the onset of summit lava terrain, dominated by lobate and sheet flows with collapsed areas. Both dives did not reach far enough west of the axis to make similar observations of a western transition from younger to older terrain (see *Alvin* tracks in bottom panels of Fig. 4).

Thus, the correlation of large magnetic gradients, seismic layer thickening profiles, and distribution limits of young lava from seafloor observations provides strong evidence for a common process that links these observations. Our conceptual framework of linking the emplacement of young highly magnetized lava together with the construction of layer 2A is shown in the forward modeling (Fig. 2). We can directly compare the observed magnetic profiles to the two end member models in Fig. 2. The profile at 9°50′N exhibits a triangular thickening profile and a more overall positive CAMH, whereas the profile at 9°31′N shows a trapezoidal thickening profile with strong flanking magnetic anomaly highs and a weaker central portion of the CAMH. The success of the forward modeling justifies the inverse approach: deconvolution of the magnetic data for lava distribution and integration of that distribution for magnetic layer thickness.

3.2. Deconvolution of AL2771 and AL2767: predicting lava deposition distribution and the architecture of 'Magnetic layer 2A'

Just as forward modeling the width and character of the CAMH in Fig. 2 involves convolution of the lava deposition distribution with the lava magnetization function, we can also carry out the inverse modeling approach, which is to deconvolve the observed magnetic moment $M(x)$ with the lava magnetization intensity function $I(x)$ to obtain the lava deposition distribution $L(x)$, or:

$$L(x) = M(x) \times I(x)^{-1} \text{ for } x \geq 0$$

Integration of $L(x)$ yields the magnetic layer thickness $T(x)$. For simplicity we assume that the magnetization intensity of the young lavas decays exponentially with age to a constant background value [25]. The results of this inverse modeling approach are shown in Fig. 5 for near-bottom magnetic profiles AL2771 and AL2767, which are then compared with seismic layer 2A thickness from nearby CDP27 and CDP31, respectively (the magnetic moment profiles were cut in half at the axis; each half was then processed separately). We solve simultaneously for zero-age lava magnetization intensity I_0, lava magnetization decay time τ, and annihilator multiplier. The annihilator represents a magnetization distribution that produces zero magnetic field, thus any number of annihilators may be added to the inversion solution for crustal magnetization. We obtain a minimum rms misfit of 31 meters between integrated deconvolution of AL2771 and CDP27 layer

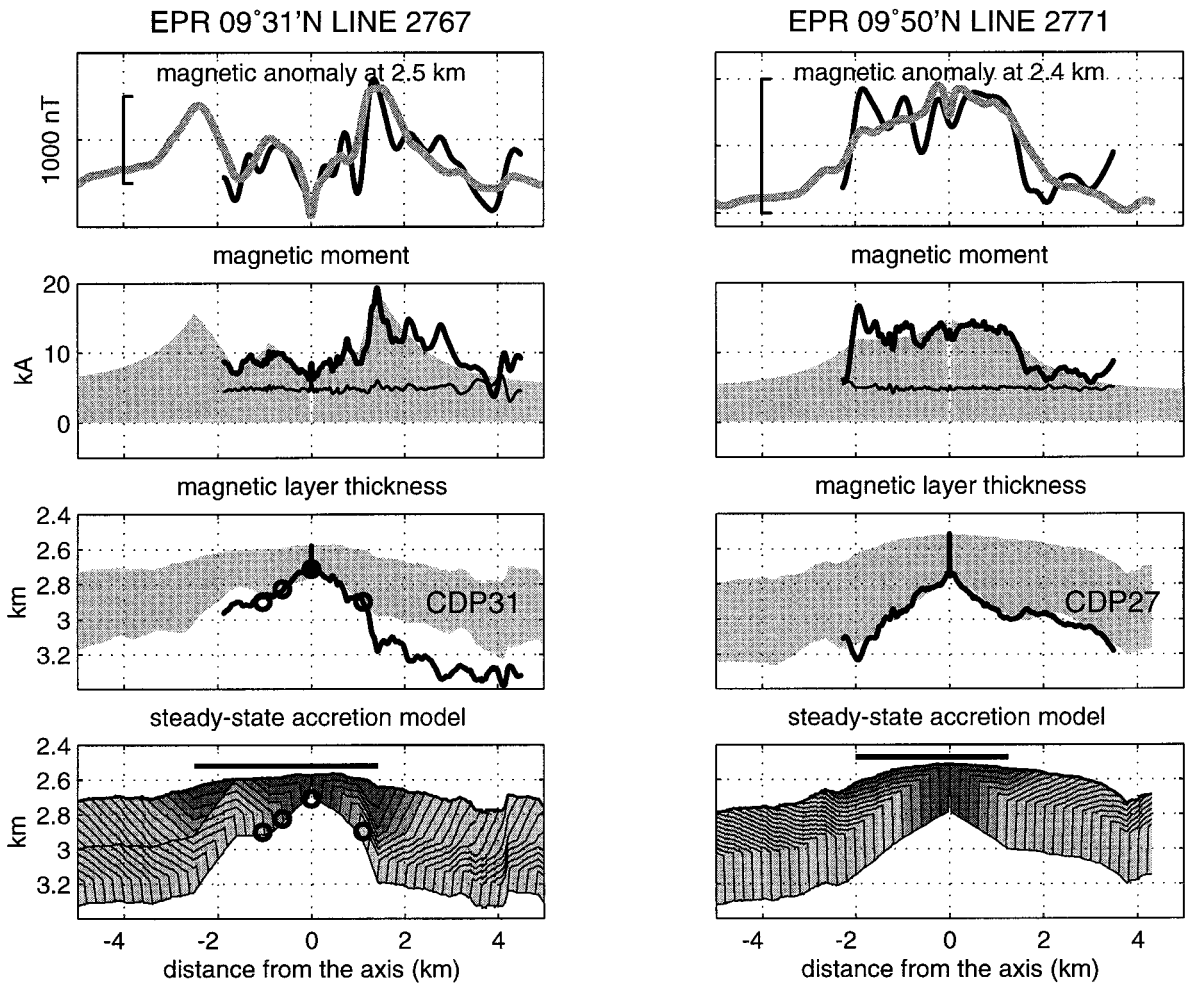

Fig. 5. Deconvolution and modeling of observed magnetic data to estimate the architecture of the magnetic source beneath near-bottom magnetic profiles AL2767 and AL2771. Description is from top to bottom. Top panels show observed magnetic anomalies from Fig. 4 (bold line) and model anomaly (shaded), calculated at 2.5 km and 2.4 km, respectively. Second row of panels shows magnetic moment (magnetization ×0.33 km) (bold line), 15 × annihilator ×0.33 km (thin line), and the model magnetic moment (shaded). Third row of panels shows nearby seismic layer 2A (shaded) and the base of the magnetic layer (bold line) obtained by deconvolution of the observed magnetic moment for lava distribution which is then integrated for magnetic layer thickness. Minimum rms misfit between the magnetic and seismic layer thicknesses in left panel is 25 m for the estimates of Christeson et al. [4] (bold circles on left) and 34 m for the central 2.5 km of CDP31 (large misfit farther off-axis due to fact that CDP31 is almost 3 km south of AL2767). Minimum rms misfit between seismic and magnetic thicknesses in right panel is 31 m. Minimization of this misfit yields an independent estimate of the lava magnetization function with a decay constant of ~20 kyr, which is identical to the function proposed by Gee and Kent [25]. Bottom panels show forward model of the magnetic layer for a steady state lava distribution. Isochrons and shading same as in Fig. 2. Horizontal bar shows extent of lava deposition and thickening of the magnetic lava layer in the model.

2A thickness (right hand panels of Fig. 5). This best-fit solution uses 30 annihilators added to the crustal magnetization solution, a zero-age lava magnetization intensity of 55 A/m and an exponential decay time of 20 kyr. The background lava magnetization intensity I_∞ was held constant at 10 A/m. Deconvolution of AL2767 with the same magnetization intensity function yields a minimum rms misfit of 25 m with the Christeson et al. [6] estimates (circles in left hand panels of Fig. 5) and 34 m with CDP31

layer 2A thickness between 1.25 km west and 1.25 km east for 32 annihilators added to the magnetization solution. We attribute the ~200 m discrepancy between off-axis thickness of AL2767 and CDP31 to the ~3 km distance between AL2767 and CDP31 (see tracks in Fig. 3) coupled with the large off-axis variability of layer 2A thickness in the region [8].

4. Discussion

The deconvolution of AL2771 with an exponential magnetization intensity function and subsequent integration (Fig. 5) provides a remarkable match to the base of seismic layer 2A in CDP27, which crosses AL2771 at the EPR axis and is not offset from the *Alvin* track by more than 1 km (see Fig. 3). A minimum rms misfit of only 31 m is obtained for a lava magnetization intensity function with $I_0 = 55$ A/m, $\tau = 20$ kyr, and $I_\infty = 10$ A/m, which is identical to the MORB magnetization function that was proposed by Gee and Kent [25]. The good match between the magnetic lava layer thickness of AL2771 and the seismic layer 2A thickness of CDP27 (right hand panels of Fig. 5) suggests that the process of generating the upper volcanic carapace at this location on the fast-spreading EPR is, to a large extent, steady state. It also implies that the layer 2A thickening with distance from the axis can be caused exclusively by the deposition of young, highly magnetic lava flows on the upper flanks of the rise at distances of up to ~2 km from the axis.

By contrast, the CAMH of AL2767 and the thickness of layer 2A in CDP31 are only qualitatively compatible (left hand panels of Fig. 5). The low magnetic moment in the central part of the profile (from ~1.5 km west to ~1.0 km east of the axis) indicates a relatively thin magnetic layer in the central 2.5 km, while the significant flanking highs suggest a rapid thickening of the magnetic layer qualitatively similar to the trapezoidal cross-section of layer 2A seen in CDP31 (the western magnetic high is inferred from the sea surface magnetic anomaly in Fig. 4). However, deconvolution of the observed CAMH and the forward modeling discussed earlier either underestimate the CDP31 thickness of layer 2A near the EPR axis or overestimate its thickness farther away. Considering that: (1) the on-axis thickness of layer 2A in the 9°–10°N region is less variable than its off-axis thickness along strike [8,9], and (2) the CDP31 line and the Christeson et al. [6] on-bottom refraction lines are respectively ~3 km and ~1.5 km south of the AL2767 track, we prefer the model where we match the observed near-field 2A thicknesses.

The magnetic lava layer thickness estimates are not absolute even if the lava magnetization intensity function were known more accurately. This is because the magnitude of the magnetic anomalies and the inferred magnetic moment are not absolute but relative to the regional field and annihilator. However, estimation by this method of the *relative* magnetic lava layer thickness near the ridge crest appears fairly insensitive to the choice of annihilator multiplier because the thickness variation depends mostly on the relative amplitude rather than on the absolute amplitude of the CAMH.

Analysis of the two near-bottom magnetic profiles and their comparison to nearby seismic observations suggest a robust relation between the CAMH and the thickening of seismic layer 2A. This relation indicates that magnetic highs, representing significant volumes of young, highly magnetic lavas, correlate with strong horizontal gradients in seismic layer 2A thickness. In profile AL2771 at 9°50′N, the CAMH extends from ~2.1 km west to ~1.5 km east of the axis while layer 2A thickens over that same distance (Fig. 4). The CAMH is relatively flat, suggesting a fairly uniform volume of young, highly magnetic lavas deposited over that range. Correspondingly, layer 2A thickness near 9°50′N increases uniformly beneath the flat CAMH, thus producing a triangular layer 2A profile (Figs. 2 and 5). In profile AL2767 at 9°31′N, the CAMH is dramatically different consisting of a broad axial low with a flanking high located at ~1.5 km east of the axis, while the other flanking high, inferred from the sea surface anomaly is located at >2.0 km west of the axis, beyond the limit of the dive (Fig. 4). Correspondingly, layer 2A near 9°31′N is relatively thin and constant under the magnetic low but thickens rapidly under the magnetic highs, which yields a trapezoidal layer 2A profile (Figs. 2 and 5).

If all lavas are erupted only at the axial summit trough, then this predicts that the lavas erupted at 9°50′N emanate in sheets along the length of the

trough to uniformly cover the crest and upper flanks of the rise. By contrast, at 9°31′N, two major lava depocenters lie at ~1.5 east and >2 km west of the axis, suggesting that the lavas erupt from the axial summit trough but are efficiently transported in lava tubes or channels to the depocenters on the upper flanks of the rise. The latter process would explain the relative slow growth of layer 2A between the axis and the off-axis depocenters at 9°31′N. The difference between the two lava deposition processes may be related to a difference in the effusion rate and or volume of erupted lavas at these two locations. The shallower rise crest and greater layer 2A thickness at 9°50′N suggest a spreading center that is magmatically more robust with greater volume of erupted lavas than at 9°31′N. Larger eruptions at 9°50′N could lead to a regular flooding of the crest and upper flanks with sheet and lobate lavas. Smaller eruptions at 9°31′N could lead to a channeling of the lavas and more efficient transport to depocenters on the flanks. If, on the other hand, the lavas on the EPR are erupted more locally and not transported over distances up to several kilometers from the axial summit trough, then this suggests relatively uniform dike injection over the width of the CAMH at 9°50′N. At 9°31′N, this could indicate that dike injection takes place at the two off-axis depocenters in addition to focused dike injection at the rise crest.

Shorter-wavelength magnetic highs, and especially the steep gradients at the edges of the CAMH, are not sufficiently accounted for by the models in Fig. 5. This may be explained by a more punctuated process of lava deposition in a number of smaller areas, too small to be resolved by seismic data. These smaller lava depocenters may exist and grow for several 10 kyrs moving farther from the axis as the seafloor spreads, and could become the source of the shorter-wavelength magnetic highs. Another explanation for the discrepancy may also be the limitations of the one-dimensional method which uses the average magnetization rather than the actual vertical distribution of magnetization in the magnetic layer and thus tends to smooth out some of the magnetization contrasts in the shallowest, youngest lavas. Lastly, there remains a possibility that older paleointensity variations also contribute to the shorter-wavelength variability of the CAMH.

5. Conclusion

The predictable structure of the CAMH at a fast-spreading MOR and our success in modeling some key features of the near-bottom CAMH lead us to believe that we can use this magnetic anomaly as an indicator for the thickness of young lavas at the MOR crest. Conceptually, we are able to attribute certain characteristics of the CAMH anomaly to volcanic emplacement processes that are active at a ridge crest, and we suggest that the CAMH anomaly provides a detailed record of the upper crustal structure and temporal and spatial evolution of the accretion process affecting segments of the MOR over the past ~50 kyr.

Our preferred model consists of a steady-state deposition of lavas at the rise crest as well as on its flanks that is responsible for the finite thickness of seismic layer 2A at the ridge axis and its rapid thickening off axis. In the ideal case, the steady-state lava deposition distribution equals the absolute value of the horizontal derivative of the thickness of the lava layer, which we assume is equivalent to seismic layer 2A. The high magnetization of young MORB lavas suggests that the extrusive layer is the prime source for CAMH anomalies. Deconvolution of the CAMH with a function that describes the decay of the initially high magnetization with time, yields a steady-state distribution of lava deposition that, after integration for magnetic layer thickness, matches the estimated nearby thickness of layer 2A.

Comparison of the magnetic and seismic layer 2A thickness provides an independent estimate of the MORB magnetization intensity function. This function, decreasing from ~55 A/m to a background value of ~10 A/m with a decay time of ~20 kyr, is identical to the estimate of Gee and Kent [25]. The rapid, 5–6 fold decrease of the MORB magnetization intensity is proportional to paleointensity and alteration decay. Since paleointensity has increased by a factor 2 over the past ~40 kyr [23], this suggests a 2–3 fold decay on a similar time scale due to low-temperature alteration. This implies that except for the recent increase of the geomagnetic field intensity, older paleointensity variations recorded in the MORB are rapidly attenuated by the effects of low-temperature alteration.

This study shows how we can use near-bottom magnetic measurements of the CAMH to estimate lava deposition and volcanic construction at a fast spreading MOR. Magnetic highs are interpreted to represent significant volumes of young, highly magnetic lavas while magnetic lows represent the relative lack thereof. Magnetic highs are found to correlate with strong horizontal gradients in the thickness of seismic layer 2A, suggesting that voluminous, active lava deposition is responsible for its thickening. Thickening of layer 2A by increasing alteration of the upper crust, or by injection with magmatic sills would decrease rather than increase its magnetization.

Our analysis suggests on-going deposition of lavas over the ~3.5–4 km width of the CAMH, which is dramatically wider than the <300 m width of axial summit trough of the 9°–10°N segment of the EPR [14]. If lava is erupted only at the axial summit trough, then this requires that a significant proportion of the lava travels several kilometers in sheets or through lava tubes or channels before deposition on the upper flanks of the rise. If, on the other hand, lava does not travel that far before deposition, then this implies that dike injection (equals seafloor spreading) and eruption are not restricted to the axial summit trough but are distributed over the width of the CAMH.

The similarity between magnetic layer and seismic layer 2A at the 9°–10°N segment of the EPR crest provides independent support to the notion that seismic layer 2A in young oceanic crust represents the highly magnetic lava layer, and that the velocity gradient at the base of layer 2A is related to the increasing number of higher-velocity dikes with depth in the lava–dike transition zone. The 4–8 km width over which layer 2A roughly doubles in thickness and a similar width of the CAMH indicate that roughly half the lavas presently erupted at the EPR are deposited outside the <300 m wide axial summit trough on the upper flanks of the rise.

Acknowledgements

We thank the officers and crew of R/V *Atlantis-II* and R/V *Atlantis*, and *Alvin* pilots and technical support team at sea and on shore of the Deep Submergence Operations Group for their dedication and assistance in helping us collect these data. We thank S. Carbotte, J. Gee and D. Wilson for constructive reviews of the manuscript, and D. Smith and T.K.P. Gregg for discussion of the data and early drafts. B. Coakley, R. Herr and T.K.P. Gregg assisted in the collection of the data at sea. This work was supported by National Science Foundation Grants: NSF-OCE8309027 (HS), NSF-OCE9505514 (MAT), NSF-OCE9408904 and NSF-OCE9505384 (DJF), NSF-OCE9314866 (JRC). WHOI Contribution 9875. ***[CL]***

References

[1] D.R. Toomey, G.M. Purdy, S.C. Solomon, W.S.D. Wilcock, The three-dimensional seismic velocity structure of the East Pacific Rise near latitude 9°30′N, Nature 347 (1990) 639–645.

[2] E.E. Vera, J.B. Diebold, Seismic imaging of oceanic layer 2A between 9°30′N and 10°N on the East Pacific Rise from two-ship wide-aperture profiles, J. Geophys. Res. 99 (1994) 3031–3041.

[3] A.J. Harding, G.M. Kent, J.A. Orcutt, A multichannel seismic investigation of the upper crustal structure at 9°N on the East Pacific Rise: Implications for crustal accretion, J. Geophys. Res. 98 (1993) 13925–13944.

[4] G.M. Kent, A.J. Harding, J.A. Orcutt, R.S. Detrick, J.C. Mutter, P. Buhl, Uniform accretion of oceanic crust south of the Garret transform at 14°15′S on the East Pacific Rise, J. Geophys. Res. 99 (1994) 9097–9116.

[5] S.M. Carbotte, J.C. Mutter, L. Xu, Contribution of volcanism and tectonism to axial and flank morphology of the southern EPR, 17°10′–17°40′S, from a study of Layer 2A geometry, J. Geophys. Res. 102 (1997) 10165–10184.

[6] G.L. Christeson, G.L. Fryer, G.M. Purdy, Seismic constraints on shallow crustal emplacement processes at the fast spreading East Pacific Rise, J. Geophys. Res. 99 (1994) 17957–17973.

[7] G.L. Christeson, W.S.D. Wilcock, G.M. Purdy, The shallow attenuation structure of the fast spreading East Pacific Rise near 9°30′N, Geophys. Res. Lett. 21 (1994) 321–324.

[8] G.L. Christeson, G.M. Kent, G.M. Purdy, R.S. Detrick, Extrusive thickness variability at the East Pacific Rise, 9°–10°N: Constraints from seismic techniques, J. Geophys. Res. 101 (1996) 2859–2873.

[9] E.E.E. Hooft, H. Schouten, R.S. Detrick, Constraining crustal emplacement processes from the variation in seismic layer 2A thickness at the East Pacific Rise, Earth Planet. Sci. Lett. 142 (1996) 289–309.

[10] S.A. Hussenoeder, G.M. Kent, R.S. Detrick, A.J. Harding, A comparison of upper crustal structure between fast

and slow spreading ridges from genetic algorithm seismic waveform inversion, Eos Trans. AGU 77 (1996) 729.
[11] R.M. Haymon, D.J. Fornari, K.L. Von Damm, M.D. Lilley, M.R. Perfit, J.M. Edmond, W.C. Shanks III, R.A. Lutz, J.M. Grebmeier, S. Carbotte, D. Wright, E. McLaughlin, M. Smith, N. Beedle, E. Olson, Volcanic eruption of the mid-ocean ridge along the East Pacific Rise crest at 9°45–52′N: Direct submersible observations of seafloor phenomena associated with an eruption event in April, 1991, Earth Planet. Sci. Lett. 119 (1993) 85–101.
[12] R.M. Haymon, The response of ridge crest hydrothermal systems to segmented, episodic magma supply in: C.J. MacLeod, P.A. Tyler, C.L. Walker (Eds.), Tectonic, Magmatic and Hydrothermal and Biological Segmentation of Mid-Ocean Ridges, Geol. Soc. London Spec. Publ. 118 (1996) 157–168.
[13] M.R. Perfit, D.J. Fornari, M.C. Smith, J.F. Bender, C.H. Langmuir, R.M. Haymon, Small-scale spatial and temporal variations in mid-ocean ridge crest magmatic processes, Geology 22 (1994) 375–379.
[14] D.J. Fornari, R.M. Haymon, M.R. Perfit, M.H. Edwards, Geological characteristics and evolution of the axial zone on fast spreading mid-ocean ridges: Formation of an axial summit trough along the East Pacific Rise, 9°–10°N, J. Geophys. Res. 103 (1998) 9827–9855.
[15] S.J. Goldstein, M.R. Perfit, R. Batiza, D.J. Fornari, M.T. Murrell, Temporal variations in East Pacific Rise magmatic activity based on U-series dating of basalts, Nature 367 (1994) 157–159.
[16] T.K.P. Gregg, D.J. Fornari, M.R. Perfit, R.M. Haymon, J.H. Fink, Rapid emplacement of a mid-ocean ridge lava flow: the East Pacific Rise at 9°46′–51′N, Earth Planet. Sci. Lett. 144 (1996) E1–E7.
[17] K.C. Macdonald, P.J. Fox, R.T. Alexander, R. Pockalny, P. Gente, Volcanic growth faults and the origin of abyssal hills on the flanks of the East Pacific Rise, Nature 380 (1996) 125–129.
[18] K.C. Macdonald, S.P. Miller, S.P. Huestis, F.N. Spiess, Three-dimensional modelling of a magnetic reversal boundary from inversion of deep-tow measurements, J. Geophys. Res. 85 (1980) 3670–3680.
[19] K.C. Macdonald, S.P. Miller, B.P. Luyendyk, T.M. Atwater, L. Shure, Investigation of a Vine Matthews magnetic lineation from a submersible: The source and character of marine magnetic anomalies, J. Geophys. Res. 88 (1983) 3403–3418.
[20] J.-C. Sempere, K.C. Macdonald, Marine tectonics: Processes at midocean ridges, Rev. Geophys. 25 (1987) 1313–1347.
[21] K.D. Klitgord, S.P. Huestis, J.D. Mudie, R.L. Parker, An analysis of near-bottom magnetic anomalies: Seafloor spreading and the magnetized layer, Geophys. J. R. Astron. Soc. 43 (1975) 387–424.
[22] M.A. Tivey, The central anomaly magnetic high: Its source and implications for ocean crust construction and evolution, Ph.D. Thesis, School of Oceanography, University of Washington, Seattle, WA, 1988, 131 pp.
[23] Y. Guyodo, J.-P. Valet, Relative variations in geomagnetic intensity from sedimentary records: the past 200,000 years, Earth Planet. Sci. Lett. 143 (1996) 23–36.
[24] K.D. Klitgord, Sea-floor spreading: the central anomaly magnetization high, Earth Planet. Sci. Lett. 29 (1976) 201–209.
[25] J. Gee, D.V. Kent, Variations in layer 2A thickness and the origin of the central anomaly magnetic high, Geophys. Res. Lett. 21 (1994) 297–300.
[26] L.J. Perram, K.C. Macdonald, S.P. Miller, Deep tow magnetics near 20°S on the East Pacific Rise: A study of short-wavelength anomalies at a very fast spreading center, Mar. Geophys. Res. 12 (1990) 235–245.
[27] M.A. Tivey, H.P. Johnson, Variations in oceanic crustal structure and the implications for the fine-scale magnetic anomaly signal, Geophys. Res. Lett. 20 (1993) 1879–1882.
[28] M.A. Tivey, H.P. Johnson, The central anomaly magnetic high: Implications for ocean crust construction and evolution, J. Geophys. Res. 92 (1987) 12685–12694.
[29] M.A. Tivey, Fine-scale magnetic anomaly field over the southern Juan de Fuca Ridge: Axial magnetization low and implications for crustal structure, J. Geophys. Res. 99 (1994) 4833–4855.
[30] H.P. Johnson, M.A. Tivey, Magnetic properties of zero-age oceanic crust: A new submarine lava flow on the Juan de Fuca Ridge, Geophys. Res. Lett. 22 (1995) 175–178.
[31] M.A. Tivey, H.P. Johnson, Alvin magnetic survey of zero-age crust: Coaxial segment eruption, Juan de Fuca Ridge 1993, Geophys. Res. Lett. 22 (1995) 171–174.
[32] H.P. Johnson, M. Hutnak, Conductive heat loss in recent eruptions at mid-ocean ridges, Geophys. Res. Lett. 24 (1997) 3089–3092.
[33] M.A. Tivey, H.P. Johnson, A. Bradley, D. Yoerger, Thickness measurements of submarine lava flows determined from near-bottom magnetic field mapping by autonomous underwater vehicle, Geophys. Res. Lett. 25 (1998) 805–808.
[34] M. Marshall, A. Cox, Magnetic changes in pillow basalt due to sea-floor weathering, J. Geophys. Res. 77 (1972) 6459–6469.
[35] E. Irving, The mid-Atlantic ridge at 45°, XIV. Oxidation and magnetic properties of basalt; review and discussion, Can. J. Earth Sci. 7 (1970) 1528–1538.
[36] H.P. Johnson, T. Atwater, Magnetic study of basalts from the Mid-Atlantic ridge, lat. 37°N, Geol. Soc. Am. Bull. 88 (1977) 637–647.
[37] H.P. Johnson, J.M. Hall, A detailed rock magnetic and opaque mineralogy study of the basalts from the Nazca plate, Geophys. J.R. Astron. Soc. 52 (1978) 45–64.
[38] J.-C. Sempere, K.C. Macdonald, Deep-tow studies of the overlapping spreading centers at 9°03′N on the East Pacific Rise, Tectonics 5 (1986) 881–900.
[39] K.C. Macdonald, Near-bottom magnetic anomalies, asymmetric spreading, oblique spreading, and tectonics of the Mid-Atlantic Ridge near lat 37°N, Geol. Soc. Am. Bull. 88 (1977) 541–555.
[40] V. Mejia, N.D. Opdyke, M.R. Perfit, Paleomagnetic field

intensity recorded in submarine basaltic glass from the East Pacific Rise, the last 69 ka, Geophys Res. Lett. 23 (1996) 475–478.
[41] J. Gee, D.A. Schneider, D.V. Kent, Marine magnetic anomalies as recorders of geomagnetic intensity variations, Earth Planet. Sci. Lett. 144 (1996) 327–335.
[42] E. Tric, J.-P. Valet, P. Tucholka, M. Paterne, L. Labeyrie, F. Guichard, L. Tauxe, M. Fortune, Paleointensity of the geomagnetic field during the last 80,000 years, J. Geophys. Res. 97 (1992) 9337–9351.
[43] J.-P. Valet, L. Meynadier, Geomagnetic field intensity and reversals during the past four million years, Nature 366 (1993) 234–238.
[44] D.A. Schneider, G.A. Mello, A high-resolution marine sedimentary record of geomagnetic paleointensity variation, Earth Planet. Sci. Lett. 144 (1996) 297–413.
[45] S.P. Miller, The validity of the geological interpretations of marine magnetic anomalies, Geophys. J. R. Astron. Soc. 50 (1977) 1–21.
[46] H. Schouten, K. McCamy, Filtering marine magnetic anomalies, J. Geophys. Res. 77 (1972) 7089–7099.
[47] C.H. Langmuir, J.F. Bender, R. Batiza, Petrologic and tectonic segmentation of the East Pacific Rise, 5°30′–14°30′N, Nature 322 (1986) 422–429.
[48] M.A. Tivey, G.M. Kent, D.J. Fornari, J.R. Cochran, Submersible magnetic profiles across the East Pacific Rise at 9°50′N and 9°30′N. Implications for Layer 2A structure, Eos Trans. AGU 75 (44) (1994) 601.
[49] J.R. Cochran, D.J. Fornari, B.J. Coakley, R. Herr, Near-bottom underway gravity study of the shallow structure of the axis of the East Pacific Rise, 9°30′N and 9°50′N, Eos Trans. AGU 77 (1996) F698.
[50] J.R. Cochran, D.J. Fornari, B.J. Coakley, R. Herr, M.A. Tivey, Continuous near-bottom gravity measurements made with a BGM-3 gravimeter in DSV Alvin on the East Pacific Rise crest near 9°30′N and 9°50′N, J. Geophys. Res. (in press).
[51] W.H. Press, B.P. Flannery, S.A. Teukolsky, W.T. Vetterling, Numerical Recipes: The Art of Scientific Computing, Cambridge University Press, Cambridge, UK, 1986, 818 pp.
[52] F. Guspi, Frequency-domain reduction of potential field measurements to a horizontal plane, Geoexploration 24 (1987) 87–98.
[53] International Association of Geomagnetism and Aeronomy (IAGA), Division V, Working Group 8, International geomagnetic reference field, 1995 revision, Geophys. J. Int. 125 (1996) 318–321.
[54] R.L. Parker, S.P. Huestis, The inversion of magnetic anomalies in the presence of topography, J. Geophys. Res. 79 (1974) 1587–1593.
[55] R.M. Haymon, D.J. Fornari, M.H. Edwards, S. Carbotte, D. Wright, K.C. Macdonald, Hydrothermal vent distribution along the East Pacific Rise crest (9°09′–54′N) and its relationship to magmatic and tectonic processes on fast-spreading mid-ocean ridges, Earth Planet. Sci. Lett. 104 (1991) 513–534.
[56] S. Carbotte, K.C. Macdonald, East Pacific Rise 8°N–10°30′N: Evolution of ridge segments and discontinuities from SeaMARC II and three-dimensional magnetic studies, J. Geophys. Res. 97 (1992) 6959–6982.